Journal of Science and Technology in Civil Engineering, HUCE, 2024, 18 (3): 1–18

FREE VIBRATION ANALYSIS OF LAMINATED COMPOSITE SHALLOW CURVED BEAM WITH VARIOUS BOUNDARY CONDITIONS

Nguyen Thien Nhan[a,b], Nguyen Ngoc Duong[a,*], Nguyen Trung Kien[c]

[a]*Faculty of Civil Engineering, Ho Chi Minh City University of Technology and Education, No. 1 Vo Van Ngan street, Thu Duc city, Ho Chi Minh city, Vietnam*
[b]*Faculty of Engineering, Kien Giang University, 320A - National Highway 61, Minh Luong Town, Chau Thanh district, Kien Giang, Vietnam*
[c]*CIRTech Institute, Ho Chi Minh City University of Technology (HUTECH), 475A Dien Bien Phu street, Binh Thanh district, Ho Chi Minh city, Vietnam*

Article history:
Received 29/5/2024, Revised 05/8/2024, Accepted 06/9/2024

Abstract

This study introduces a novel Ritz approximation function to analyze the free vibrations of laminated composite shallow curved beams. The methodology utilizes polynomial functions-based Fibonacci series to develop the Ritz's approximation function. The displacement field aligns with the high-order shear deformation theory designed explicitly for shallow curved beams. The problem's governing equation is established by applying the Lagrange equation, providing a comprehensive framework for the subsequent analysis. The study meticulously examines the convergence rate and accuracy of the proposed approximation function. Numerical investigations are conducted to determine the natural frequencies of curved beams. Factors such as curvature-to-length ratio, length-to-thickness ratio, boundary conditions, and material anisotropy are carefully considered. Furthermore, extensive survey results concerning the natural frequencies of curved beams are presented. These results serve as valuable reference data for future investigations in this area, thereby contributing to the academic discourse on this subject matter.

Keywords: laminated composite shallow curved beam; free vibration; Ritz method; high-order shear deformation beam theory.

https://doi.org/10.31814/stce.huce2024-18(3)-01

1. Introduction

The increased utilization of multilayered materials in numerous engineering applications could be attributed to their high strength-to-weight ratio, high stiffness-to-weight ratio, fatigue resistance, and customization capability to fulfill specific design requirements for strength and stiffness. Various engineering structures, such as aircraft wings, helicopter blades, and roofs, are often represented as curved beams. As a result, many researchers have been simulating the behaviors of laminated composite curved beams. Understanding the free vibration characteristics, encompassing the natural frequencies and mode shapes, is crucial for laminated composite curved beams exposed to dynamic loads. Accurately portraying laminated beams' dynamic characteristics requires adopting a suitable mathematical model in conjunction with an appropriate solution method. Several beam models and methods have been developed to assess laminated composite curved beams' free vibration characteristics [1, 2].

The classical beam theory (CBT) [3, 4] serves as the fundamental framework for beam analysis. However, CBT overlooks shear deformation effects, rendering it most suitable for analyzing thin

*Corresponding author. *E-mail address:* duongnn@hcmute.edu.vn (Duong, N. N.)

beams. Adapting to the analysis of thick beams, the first-order shear deformation beam theory (FSDBT) [5–8] introduces a shear correction factor. Furthermore, the higher-order shear deformation beam theory (HSDBT) emerges as a comprehensive alternative for thick beam analysis, garnering significant interest from the research community [9–15]. Numerical methods like the finite element method (FEM) [16–19] and isogeometric analysis [20, 21] have been used for analyzing curved beams. Besides, analytical methods such as Navier's solution [22–24] specifically apply to simply-supported beams. The analytical prowess of the Ritz method [25–28] highlights the critical role of choosing suitable approximation functions for accuracy and convergence. Each theoretical framework and analysis method exhibits distinct advantages and constraints, capturing the attention of scholars in recent years. Noteworthy research includes the analysis of functionally graded material (FGM) curved beams by Karamanli et al. [29] and the exploration of composite curved beams' free vibration using the HSDBT theory and FEM approach by Marur and Kant [30]. Qatu and Elsharkawy [31] delved into the implementation of the Ritz method, employing polynomial approximation functions for analyzing the free vibration of curved beams based on FSDBT theory under various boundary conditions. Further investigations encompassed the study of free vibration in FG curved beams by Yousefi and Rastgoo [32] utilizing the Ritz method with Jacobi polynomial approximations. Notably, FEM based on HSDBT has been introduced for delving into the behavioral characteristics of FGM curved beams in recent studies [29, 33].

After reviewing the existing literature, it is evident that exploring the free vibration of laminated composite shallow curved beams (LCSCB) utilizing the Ritz method based on the higher-order shear deformation beam theory is relatively limited. This paper aims to address this gap by introducing a novel approximation function. The proposed function is based on applying the Fibonacci series within the Ritz method to analyze the free vibration characteristics of LCSCB. The governing equation is obtained from the Lagrange's equation. The numerical results are meticulously compared with existing solutions in the literature. This comparative analysis encompasses various aspects, such as lay-up, material orthotropy ratios, length-to-thickness ratios, curvature ratios, and boundary conditions, contributing to a comprehensive understanding of the free vibration behavior of LCSCB.

2. Formulation

2.1. Kinematics

The characteristics of an LCSCB are defined by its cross-sectional dimensions illustrated in Fig. 1, where h represents the thickness, b signifies the width of the cross-section, and L denotes the length of the beam. The displacement field is based on the higher-order deformation beam theory [12]:

$$u(x,z,t) = \left(1 + \frac{z}{R}\right) u_0(x,t) - z w_{0,x}(x,t) + f(z)\phi_0(x,t) \tag{1}$$

$$w(x,z,t) = w_0(x,t) \tag{2}$$

where the displacements of the mid-surface of the LCSCB in the x- and z-directions are denoted as $u_0(x,t)$ and $w_0(x,t)$, respectively. Additionally, $\phi_0(x,t)$ represents the rotation of a transverse normal about the y-axis, while $f(z) = \frac{5z}{4} - \frac{5z^3}{3h^2}$ denotes the shear function. Furthermore, R denotes the radius of curvature.

The strain field is presented as follows:

$$\varepsilon_{xx} = u_{,x} + \frac{w}{R} = u_{0,x} - z w_{0,xx} + f\phi_{0,x} + \frac{w_0}{R} \tag{3}$$

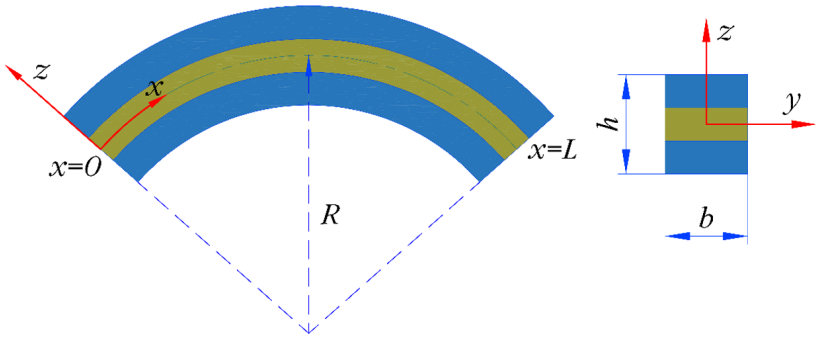

Figure 1. Geometry of curved beam

$$\gamma_{xz} = u_{,z} + w_{,x} - \frac{u_0}{R} = f_{,z}\phi_0 \tag{4}$$

It is stated that the term z/R is small in comparison with unity and hence its effect in Eq. (3) has been neglected for shallow curved beams [12, 14, 34].

2.2. Constitutive relations

The composite beam investigated in this research is a multi-layered one characterized by orthotropic behavior within each layer, exhibiting distinct fiber orientations. The stress-strain relationship for a specific layer, expressed in the global coordinate system, is mathematically represented as follows:

$$\begin{Bmatrix} \sigma_{xx}^{(k)} \\ \sigma_{xz}^{(k)} \end{Bmatrix} = \begin{Bmatrix} \bar{Q}_{11}^{(k)} & 0 \\ 0 & \bar{Q}_{55}^{(k)} \end{Bmatrix} \begin{Bmatrix} \varepsilon_{xx}^{(k)} \\ \gamma_{xz}^{(k)} \end{Bmatrix} \tag{5}$$

where $\bar{Q}_{11}^{(k)}$ and $\bar{Q}_{55}^{(k)}$ are the transformed reduced stiffness constants of the k^{th} layer, see Ref. [14] for more details.

2.3. Variational formulation

The strain energy of the beam is expressed as follows:

$$\begin{aligned} \Pi_{SE} &= \frac{1}{2}\int_V (\sigma_{xx}\varepsilon_{xx} + \sigma_{xz}\gamma_{xz})dV \\ &= \frac{1}{2}\int_0^L \begin{pmatrix} Au_{0,x}^2 - 2Bu_{0,x}w_{0,xx} + Dw_{0,xx}^2 + 2B^s u_{0,x}\phi_{0,x} - 2D^s w_{0,xx}\phi_{0,x} + H^s\phi_{0,x}^2 \\ + A^s\phi_0^2 + \frac{A}{R^2}w_0^2 + \frac{2A}{R}u_{0,x}w_0 - \frac{2B}{R}w_{0,xx}w_0 + \frac{2B^s}{R}\phi_{0,x}w_0 \end{pmatrix} dx \end{aligned} \tag{6}$$

where

$$(A, B, D, B^s, D^s, H^s) = \sum_{k=1}^{n}\int_{z_k}^{z_{k+1}} \bar{Q}_{11}^{(k)}\left(1, z, z^2, f, fz, f^2\right) bdz \tag{7}$$

$$A^s = \sum_{k=1}^{n}\int_{z_k}^{z_{k+1}} \bar{Q}_{55}^{(k)} f_{,z}^2 bdz \tag{8}$$

The kinetic energy of the beam is written as follows:

$$\begin{aligned}\Pi_{KE} &= \frac{1}{2}\int_V \left[\rho(z)\left(\dot{u}^2+\dot{w}^2\right)\right]dV \\ &= \frac{1}{2}\int_V \left[\rho(z)\begin{pmatrix}\dot{u}_0^2 - 2z\dot{u}_0\dot{w}_{0,x} + z^2\dot{w}_{0,x}^2 + 2f\dot{u}_0\dot{\phi}_0 - 2zf\dot{w}_{0,x}\dot{\phi}_0 + f^2\dot{\phi}_0^2 + \dot{w}_0^2 \\ + \frac{2z}{R}\dot{u}_0^2 + \frac{z^2}{R^2}\dot{u}_0^2 - \frac{2z^2}{R}\dot{u}_0\dot{w}_{0,x} + \frac{2zf}{R}\dot{u}_0\dot{\phi}_0\end{pmatrix}\right]dV \\ &= \frac{1}{2}\int_0^L \left[\begin{matrix}I_0\dot{u}_0^2 - 2I_1\dot{u}_0\dot{w}_{0,x} + I_2\dot{w}_{0,x}^2 + 2J_1\dot{u}_0\dot{\phi}_0 - 2J_2\dot{w}_{0,x}\dot{\phi}_0 + K_2\dot{\phi}_0^2 + I_0\dot{w}_0^2 \\ + \left(\frac{2I_1}{R} + \frac{I_2}{R^2}\right)\dot{u}_0^2 - \frac{2I_2}{R}\dot{u}_0\dot{w}_{0,x} + \frac{2J_2}{R}\dot{u}_0\dot{\phi}_0\end{matrix}\right]dx\end{aligned} \tag{9}$$

where

$$(I_0, I_1, I_2, J_1, J_2, K_2) = \sum_{k=1}^{n}\int_{z_k}^{z_{k+1}} \rho\left(1, z, z^2, f, zf, f^2\right)bdz \tag{10}$$

The total energy of the beam

$$\Pi = \Pi_{SE} - \Pi_{KE} \tag{11}$$

2.4. Method

The Ritz method is employed to approximate the displacement field in this paper as follows:

$$u_0(x,t) = \sum_{j=1}^{m} u_{0j}\psi_j e^{i\omega t} \tag{12}$$

$$w_0(x,t) = \sum_{j=1}^{m} w_{0j}\varphi_j e^{i\omega t} \tag{13}$$

$$\phi_0(x,t) = \sum_{j=1}^{m} \phi_{0j}\xi_j e^{i\omega t} \tag{14}$$

where ω is natural frequency; $i^2 = -1$; $u_{0j}, w_{0j}, \phi_{0j}$ are unknown parameters; $\psi_j(x), \varphi_j(x), \xi_j(x)$ are the approximation functions, shown in Table 1. The choice of the approximation functions significantly impacts on the convergence rate and accuracy of the solution. Presently, extensive research exists on beam analysis utilizing the Ritz method with various approximation functions, including the Chebyshev function [35] and the Hybrid function [36]. In this study, the Fibonacci sequence (FBN) [37–39] is employed for constructing the approximation functions. The FBNs, as indicated in Eq. (11), are specifically tailored to accommodate a range of boundary conditions such as simply-supported (S-S), clamped-free (C-F), clamped-simply supported (C-S), and clamped-clamped (C-C), as elaborated in Table 1.

The Fibonacci sequence is defined:

$$F_n = \begin{cases}1 & n = 0 \\ 1 & n = 1 \\ F_{n-1} + F_{n-2} & n \geq 2\end{cases} \tag{15}$$

where n are natural numbers. Developing the approximation functions from the FBN involves defining fundamental functions as follows:

$$\zeta_j(x) = \prod_{k=1}^{j}\left(\frac{F_k - 1}{F_j} - \frac{x}{L}\right) \times \prod_{k=1}^{s}\left(P_k - \frac{x}{L}\right) \tag{16}$$

$$\varpi_j(x) = \prod_{k=1}^{j}\left(\frac{F_k - 1}{F_j} - \frac{x}{L}\right) \times \prod_{k=1}^{r}\left(Q_k - \frac{x}{L}\right) \tag{17}$$

where F_k denotes the Fibonacci sequence; s, r are natural numbers, and P_k, Q_k are vectors to conform with boundary conditions as shown in Table 1.

Table 1. The approximate functions and essential boundary conditions

BCs	s	r	**P**	**Q**	$\varphi_j(x)$	$\psi_j(x)$	$\xi_j(x)$	$x = 0$	$x = L$
S-S	1	0	1	0	$\zeta_j(x)$	$\zeta_{j,x}$	$\zeta_{j,x}$	$w_0 = 0$	$w_0 = 0$
C-F	1	0	0	0	$\zeta_j(x)$	$\varpi_j(x)$	$\varpi_j(x)$	$w_0 = 0$ $u_0 = 0$ $w_{0,x} = 0$ $\phi_0 = 0$	-
C-S	2	1	(0,1)	0	$\zeta_j(x)$	$\varpi_j(x)$	$\varpi_j(x)$	$w_0 = 0$ $u_0 = 0$ $w_{0,x} = 0$ $\phi_0 = 0$	$w_0 = 0$
C-C	3	1	(0,1,1)	1	$\zeta_j(x)$	$\varpi_j(x)$	$\varpi_j(x)$	$w_0 = 0$ $u_0 = 0$ $w_{0,x} = 0$ $\phi_0 = 0$	$w_0 = 0$ $u_0 = 0$ $w_{0,x} = 0$ $\phi_0 = 0$

From Eqs. (11)–(15), and using the Lagrange's equations as follows,

$$\frac{\partial \Pi}{\partial u_{0j}} - \frac{d}{dt}\frac{\partial \Pi}{\partial \dot{u}_{0j}} = 0 \tag{18}$$

$$\frac{\partial \Pi}{\partial w_{0j}} - \frac{d}{dt}\frac{\partial \Pi}{\partial \dot{w}_{0j}} = 0 \tag{19}$$

$$\frac{\partial \Pi}{\partial \phi_{0j}} - \frac{d}{dt}\frac{\partial \Pi}{\partial \dot{\phi}_{0j}} = 0 \tag{20}$$

the characteristic equations for vibration analysis of the LCSCB can be obtained:

$$\left(\mathbf{K} - \omega^2 \mathbf{M}\right)\mathbf{q} = \mathbf{0} \tag{21}$$

where $\mathbf{q} = \begin{bmatrix}\mathbf{u}_0 & \mathbf{w}_0 & \Phi_0\end{bmatrix}^T$ is the column vector of unknown parameters, and $\mathbf{K}$ and $\mathbf{M}$ are the stiffness and mass matrix, respectively. The components of $\mathbf{K}$ and $\mathbf{M}$ are given by:

$$K_{ij}^{11} = A\int_0^L \psi_{i,x}\psi_{j,x}dx \tag{22}$$

$$K_{ij}^{12} = -B\int_0^L \psi_{i,x}\varphi_{j,xx}dx + \frac{A}{R}\int_0^L \psi_{i,x}\varphi_j dx \tag{23}$$

$$K_{ij}^{13} = B^s\int_0^L \psi_{i,x}\xi_{j,x}dx \tag{24}$$

$$K_{ij}^{22} = D\int_0^L \varphi_{i,xx}\varphi_{j,xx}dx + \frac{A}{R^2}\int_0^L \varphi_i\varphi_j dx - \frac{B}{R}\left(\int_0^L \varphi_{i,xx}\varphi_j dx + \int_0^L \varphi_i\varphi_{j,xx}dx\right) \tag{25}$$

$$K_{ij}^{23} = -D^s\int_0^L \varphi_{i,xx}\xi_{j,x}dx + \frac{B^s}{R}\int_0^L \varphi_i\xi_{j,x}dx \tag{26}$$

$$K_{ij}^{33} = H^s\int_0^L \xi_{i,x}\xi_{j,x}dx + A^s\int_0^L \xi_i\xi_j dx \tag{27}$$

$$M_{ij}^{11} = \left(I_0 + \frac{2I_1}{R} + \frac{I_2}{R^2}\right)\int_0^L \psi_i\psi_j dx \tag{28}$$

$$M_{ij}^{12} = \left(-I_1 - \frac{I_2}{R}\right)\int_0^L \psi_i\varphi_{j,x}dx \tag{29}$$

$$M_{ij}^{13} = \left(J_1 + \frac{J_2}{R}\right)\int_0^L \psi_i\xi_j dx \tag{30}$$

$$M_{ij}^{22} = I_0\int_0^L \varphi_i\varphi_j dx + I_2\int_0^L \varphi_{i,x}\varphi_{j,x}dx \tag{31}$$

$$M_{ij}^{23} = -J_2\int_0^L \varphi_{i,x}\xi_j dx \tag{32}$$

$$M_{ij}^{33} = K_2\int_0^L \xi_i\xi_j dx \tag{33}$$

3. Numerical examples

In this section, numerical examples illustrate the convergence and precision of the present method. Shallow curved beams exhibit a geometric configuration, as illustrated in Fig. 1, featuring cross-sectional dimensions of $h = b = 0.254m$. The composite material employed in this study has the following mechanical characteristics: $E_2 = 6.9\times10^9$ Pa, $E_1 = 40E_2, G_{23} = 0.5E_2, G_{12} = G_{13} = 0.6E_2$, $\rho = 1550$ kg/m^3, $\nu_{12} = 0.25$ [14].

3.1. Convergence study

This section analyzes the current approach in convergence characteristics, focusing on the LCSCB under different boundary conditions, including S-S, C-F, C-S, and C-C. The frequencies of beams corresponding to the first five mode shapes are presented in Table 2. The graphical representation in Figs. 2(a), (b), (c), and (d) illustrates the variation of $\Delta\omega^{(m)}$ with respect to m. It is noted that $\Delta\omega^{(m)}$ is defined $\Delta\omega^{(m)} = \dfrac{\left|\omega^{(m)} - \omega^{(ref)}\right|}{\omega^{(m)}} \times 100\%$ where $\omega^{(m)}$ is natural frequency of beams at m, and $\omega^{(ref)}$ is reference frequency. These results demonstrate a gradual convergence trend as the number of series (m) increases. The findings highlight the efficient and precise convergence achieved by the proposed Ritz method compared to the outcomes presented by June et al. [14], which relied on the dynamic stiffness matrix approach. Utilizing an approximation function derived from the Fibonacci series satisfies essential boundary conditions and maintains a simple structure, facilitating the process of programming formulations. In contrast, the dynamic stiffness matrix method encounters numerous challenges attributable to its intricate nature of expressions. Notably, at $m = 10$, the outcomes exhibit satisfactory precision across the boundary conditions, indicating the suitability of this point for the subsequent numerical illustrations in this study.

Table 2. Convergence study for first five frequencies ω (Hz) of LCSCBs ($L/h = 5$, $R/L = 5$, $0°/90°$) with respect to m

BCs	Mode	m						Jun et al. [14]
		2	4	6	8	10	12	
S-S	1	364.4	325.6	325.5	325.5	325.5	325.5	325.5
	2	1096.6	970.5	968.3	968.3	968.3	968.3	968.3
	3	2555.9	2010.1	1702.4	1689.6	1689.4	1689.4	1689.4
	4	4148.6	2435.6	2435.3	2435.3	2435.3	2435.3	2435.3
	5	6165.3	3203.4	2507.9	2461.9	2460.5	2460.5	2460.5
C-F	1	128.7	125.4	125.2	125.1	125.1	125.1	125.1
	2	897.7	585.1	578.5	577.4	577.3	577.3	577.3
	3	1699.3	1281.1	1253.5	1250.1	1249.6	1249.5	1249.6
	4	3379.6	1689.4	1661.2	1660.0	1659.9	1659.9	1659.9
	5	3842.5	2956.0	2089.3	2054.8	2052.4	2052.3	2052.4
C-S	1	489.3	429.5	426.3	425.6	425.5	425.5	425.5
	2	1628.9	1069.4	1059.8	1057.0	1056.7	1056.7	1056.7
	3	3341.4	1627.3	1627.1	1627.1	1627.1	1627.1	1627.1
	4	3610.3	2292.4	1789.2	1781.2	1780.0	1779.9	1780
	5	3908.2	3013.9	2618.6	2570.1	2564.6	2564.5	2564.6
C-C	1	581.2	570.9	568.8	568.6	568.5	568.5	568.5
	2	2429.5	1154.2	1144.0	1140.5	1140.1	1140.1	1140.1
	3	3646.9	1894.8	1879.3	1875.6	1875.4	1875.4	1875.4
	4	3913.6	2431.9	2425.2	2424.7	2424.6	2424.6	2424.6
	5	5784.3	3589.0	2738.3	2694.7	2687.7	2687.7	2687.7

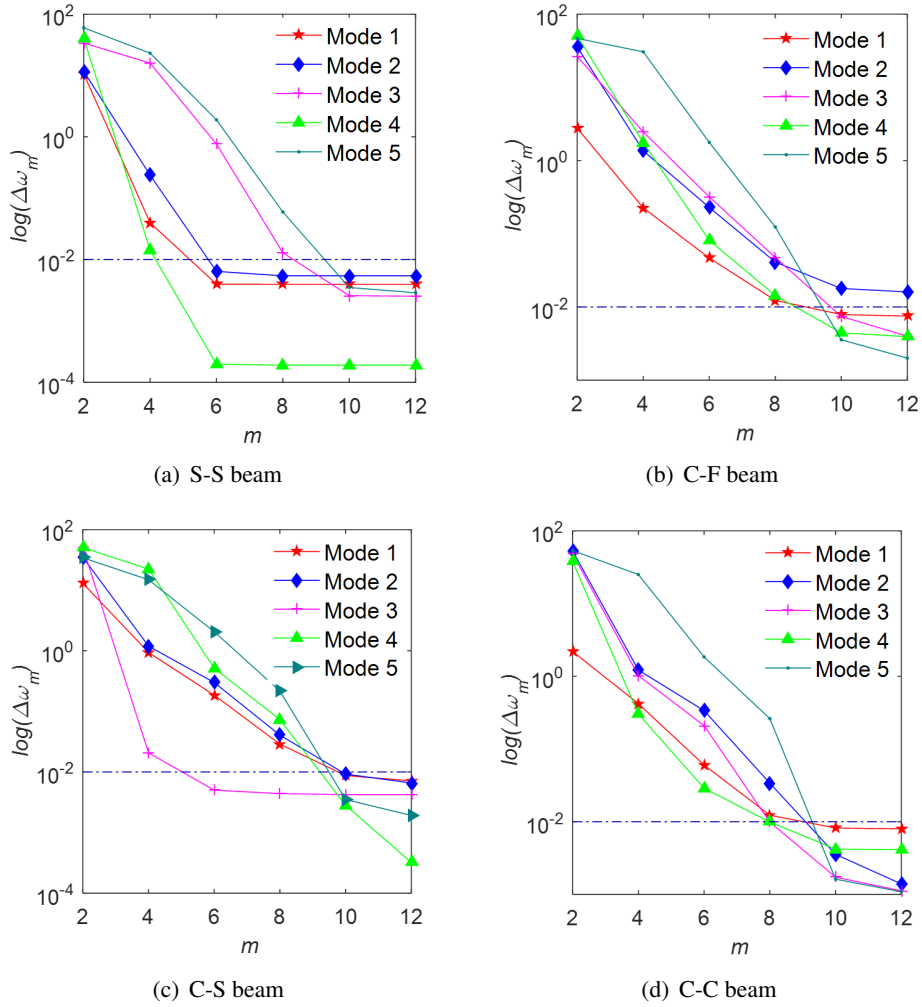

(a) S-S beam (b) C-F beam

(c) C-S beam (d) C-C beam

Figure 2. Convergence rate for first five frequencies of LCSCB with various boundary conditions

3.2. Verification study

The research outcomes for $(0^\circ/90^\circ)$ and $(0^\circ/90^\circ/0^\circ)$; LCSCBs $(R/L = 5)$ across various boundary conditions are detailed in Table 3. A comparative analysis of the first five natural frequencies with the results obtained by Jun et al. [14], employing the HSDBT and dynamic stiffness matrix, reveals a correlation between the findings of this study and those of Ref. [14]. Additionally, the examination delves into the non-dimensional fundamental frequencies of $(0^\circ/90^\circ)$ and $(0^\circ/90^\circ/0^\circ)$ beams for various length-to-thickness and curvature ratios under diverse boundary conditions, as presented in Tables 4 and 5. Notably, the findings demonstrate that the present results and those of Khdeir and Reddy [12], who utilized HSDBT and the state space solution, are consistent.

Besides, the free vibration response of beams with arbitrary angles is investigated. The present results are presented in Table 6 and compared with those of Mantari and Canales [27] which HSDBT theory and Ritz method based on hybrid functions are used. It is seen that the present results are in agreement with those of Ref. [27]. These instances serve to substantiate the soundness of the current formulation.

Table 3. First five frequencies ω (Hz) of LCSCBs ($R/L = 5$)

BCs	Reference	Mode				
		ω_1	ω_2	ω_3	ω_4	ω_5
$0^\circ/90^\circ, L/h = 10$						
S-S	Present	92.0	325.0	629.8	967.1	1324.6
	Jun et al. [14]	92.0	325.0	629.8	967.1	1321.6
C-F	Present	33.5	186.9	452.6	769.9	914.0
	Jun et al. [14]	33.4	186.8	452.4	769.5	913.9
C-S	Present	133.8	376.3	678.2	910.9	1013.1
	Jun et al. [14]	133.8	376.2	677.9	910.8	1012.5
C-C	Present	207.1	425.9	726.7	1056.6	1409.1
	Jun et al. [14]	207.1	425.7	726.4	1055.9	1408.7
$0^\circ/90^\circ/0^\circ, L/h = 5$						
S-S	Present	486.0	1132.3	1848.3	2676.4	3651.3
	Jun et al. [14]	486.0	1132.3	1848.3	2676.4	3059.8
C-F	Present	223.2	763.1	1505.7	2168.3	2287.4
	Jun et al. [14]	223.1	763.0	1505.6	2168.2	2287.4
C-S	Present	538.4	1204.5	1954.3	2178.1	2830.0
	Jun et al. [14]	538.4	1204.4	1954.3	2178.1	2829.9
C-C	Present	657.5	1283.6	2081.8	2991.3	4051.7
	Jun et al. [14]	657.5	1283.6	2081.8	2991.1	4050.8

Table 4. Dimensionless fundamental frequencies $\left(\bar{\omega} = \omega L^2/h\sqrt{\rho/E_2}\right)$ of LCSCBs ($R/L = 5$)

BCs	Reference	L/h				
		5	10	20	50	100
$0^\circ/90^\circ$						
S-S	Present	6.155	6.961	7.221	7.295	7.303
	Khdeir and Reddy [12]	6.156	6.961	-	7.294	7.303
C-F	Present	2.366	2.531	2.582	2.598	2.601
C-S	Present	8.047	10.123	11.024	11.325	11.368
	Khdeir and Reddy [12]	8.047	10.121	-	11.324	11.367
C-C	Present	10.751	15.668	21.750	40.284	45.447
	Khdeir and Reddy [12]	10.751	15.667	-	40.282	45.441
$0^\circ/90^\circ/0^\circ$						
S-S	Present	9.190	13.586	16.305	17.427	17.608
	Khdeir and Reddy [12]	9.190	13.586	-	17.427	17.608
C-F	Present	4.220	5.481	6.055	6.254	6.285

BCs	Reference	L/h				
		5	10	20	50	100
C-S	Present	10.181	16.507	22.739	26.544	27.269
	Khdeir and Reddy [12]	10.181	16.505	-	26.535	27.266
C-C	Present	12.433	21.670	34.585	57.372	93.369
	Khdeir and Reddy [12]	12.433	21.670	-	57.370	93.363

Table 5. Dimensionless fundamental frequencies $\left(\bar{\omega} = \omega L^2/h\sqrt{\rho/E_2}\right)$ of LCSCBs ($L/h = 10$)

BCs	Reference	R/L				
		5	10	20	50	∞
$0°/90°$						
S-S	Present	6.961	6.956	6.952	6.948	6.945
	Khdeir and Reddy [12]	6.961	6.956	-	-	6.945
C-F	Present	2.531	2.538	2.541	2.542	2.543
C-S	Present	10.123	10.140	10.139	10.135	10.131
	Khdeir and Reddy [12]	10.121	10.138	-	-	10.130
C-C	Present	15.668	14.194	13.798	13.684	13.661
	Khdeir and Reddy [12]	15.667	14.193	-	-	13.660
$0°/90°/0°$						
S-S	Present	13.586	13.607	13.612	13.613	13.614
	Khdeir and Reddy [12]	13.586	13.607	-	-	13.614
C-F	Present	5.481	5.490	5.493	5.493	5.494
C-S	Present	16.507	16.577	16.595	16.599	16.600
	Khdeir and Reddy [12]	16.505	16.575	-	-	16.599
C-C	Present	21.670	20.221	19.841	19.733	19.712
	Khdeir and Reddy [12]	21.670	20.221	-	-	19.712

Table 6. Dimensionless fundamental frequencies $\left(\bar{\omega} = \omega L^2/h\sqrt{\rho/E_2}\right)$ of LCSCBs ($L/h = 5, R/L = \infty$)

BCs	Reference	Lay-up					
		$0°/30°/0°$	$0°/45°/0°$	$0°/60°/0°$	$0°/30°/-30°/0°$	$0°/45°/45°/0°$	$0°/60°/-60°/0°$
S-S	Present	9.4651	9.3802	9.2947	9.4195	9.2930	9.1700
	Mantari and Canales [27]	9.4651	9.3801	9.2946	9.4194	9.2928	9.1699
C-F	Present	4.3326	4.2961	4.2624	4.2925	4.2229	4.1645
	Mantari and Canales [27]	4.3218	4.2855	4.2519	4.2821	4.2129	4.1548
C-S	Present	10.5604	10.4512	10.3440	10.5018	10.3339	10.1714
	Mantari and Canales [27]	10.8520	10.7411	10.6304	10.8021	10.6395	10.4777
C-C	Present	11.9977	11.8603	11.7284	11.9186	11.6991	11.4902
	Mantari and Canales [27]	11.8724	11.7378	11.6087	11.7949	11.5797	11.3749

3.3. Parametric analysis

The natural frequency of laminated composite shallow curved beams is investigated in this section, focusing on the effects of the length-to-thickness and curvature ratio, fiber angle, boundary condition, and material anisotropy. Fundamental frequency data for curved beams under various L/h ratios, boundary conditions (BCs), and lay-ups are presented in Tables 7 and 8. Additionally, Figs. 3(a) and 3(b) depict the fundamental frequency of (0°/45°) and (0°/45°/0°) LCSCBs ($R/L = 5$) with respect to the L/h ratio. The results illustrate a decrease in frequency with an increase in the L/h ratio and fiber angle (θ), indicating that higher L/h and θ values correspond to reduced beam stiffness. Furthermore, the analysis reveals that, for identical L/h ratios and fiber angles, the fundamental frequency is highest for C-C beams and lowest for C-F beams. This trend suggests that the constraint of BCs contributes to an augmentation in beam stiffness.

Table 7. Fundamental frequencies ω (Hz) of LCSCBs ($R/L = 5$) with one or two layers

L/h	Laminated	S-S	C-F	C-S	C-C
5	0°	504.006	230.572	561.133	703.173
	30°	450.978	196.520	512.888	632.444
	45°	371.541	151.719	446.656	552.805
	60°	250.945	95.382	336.522	436.522
	90°	142.873	52.274	209.690	290.920
	0°/30°	478.071	212.697	538.369	669.599
	0°/45°	438.389	186.507	508.899	636.882
	0°/60°	375.845	150.238	464.935	599.807
	0°/90°	325.513	125.110	425.537	568.547
10	0°	184.733	74.244	225.868	306.955
	30°	152.765	59.166	196.889	266.877
	45°	113.595	42.436	156.747	216.395
	60°	68.881	25.012	101.911	146.561
	90°	37.108	13.316	56.831	84.178
	0°/30°	167.839	65.936	211.283	287.467
	0°/45°	143.634	54.762	189.509	263.703
	0°/60°	112.305	41.485	157.558	231.608
	0°/90°	92.022	33.463	133.826	207.139

Table 8. Fundamental frequencies ω (Hz) of LCSCBs ($R/L = 5$) with three or four layers

L/h	Lay-up	S-S	C-F	C-S	C-C
5	0°/30°/0°	499.532	228.496	555.298	688.058
	0°/45°/0°	495.047	226.569	549.536	675.261
	0°/60°/0°	490.534	224.791	543.884	665.002
	0°/90°/0°	485.976	223.158	538.374	657.461
	0°/30°/-30°/0°	497.120	226.385	552.195	680.081
	0°/45°/-45°/0°	490.443	222.711	543.317	660.048
	0°/60°/-60°/0°	483.952	219.627	534.738	643.884
	0°/90°/0°/90°	411.853	174.994	474.421	587.939

L/h	Lay-up	S-S	C-F	C-S	C-C
10	0°/30°/0°	183.213	73.637	223.844	299.853
	0°/45°/0°	181.857	73.138	221.898	294.020
	0°/60°/0°	180.661	72.746	220.027	289.542
	0°/90°/0°	179.615	72.461	218.228	286.487
	0°/30°/-30°/0°	181.215	72.572	222.220	296.083
	0°/45°/-45°/0°	178.298	71.261	218.885	287.099
	0°/60°/-60°/0°	176.029	70.341	215.905	280.244
	0°/90°/0°/90°	135.000	51.462	177.827	245.133

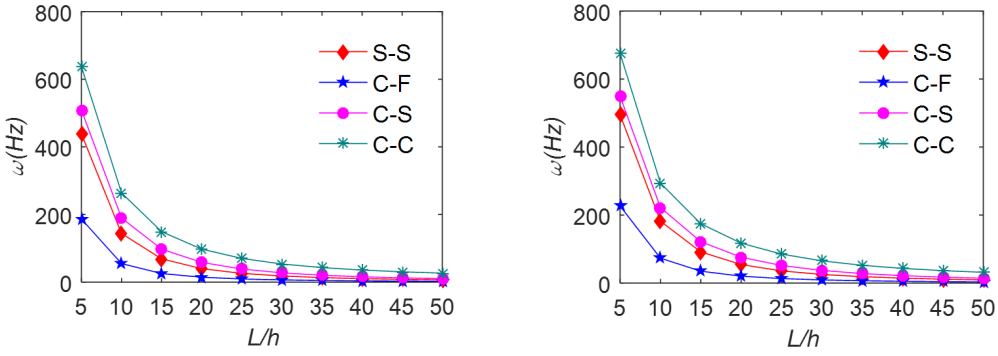

(a) (0°/45°) beam (b) (0°/45°/0°) beam

Figure 3. Fundamental frequencies ω (Hz) of the (0°/45°) and (0°/45°/0°) LCSCBs ($R/L = 5$) with respect to L/h ratio with various boundary conditions

The findings from Table 9 indicate that the fundamental frequency of LCSCBs ($L/h = 10$) remains relatively stable across various R/L ratios, suggesting that the variation in this ratio does not significantly impact the beam frequency. Furthermore, there is a discernible decrease in frequency with an increase in the fiber angle, aligning with the anticipated trend.

Table 9. Fundamental frequencies ω (Hz) of LCSCBs ($L/h = 10$) with various R/L ratios

BCs	Lay-up						
	0°	[15°/−15°]	[30°/−30°]	[45°/−45°]	[60°/−60°]	[75°/−75°]	[90°/−90°]
$R/L = 5$							
S-S	184.733	176.829	152.765	113.595	68.881	41.088	37.108
C-F	74.244	70.379	59.166	42.436	25.012	14.760	13.316
C-S	225.868	218.915	196.889	156.747	101.911	62.719	56.831
C-C	306.955	296.831	266.877	216.395	146.561	92.611	84.178
$R/L = 10$							
S-S	185.011	177.095	152.994	113.765	68.984	41.149	37.163
C-F	74.372	70.498	59.263	42.502	25.050	14.782	13.336
C-S	226.813	219.830	197.706	157.384	102.313	62.963	57.051
C-C	280.283	272.769	249.408	206.412	141.907	90.162	81.996

BCs	Lay-up						
	0°	[15°/ − 15°]	[30°/ − 30°]	[45°/ − 45°]	[60°/ − 60°]	[75°/ − 75°]	[90°/ − 90°]
$R/L = \infty$							
S-S	185.104	177.184	153.071	113.822	69.019	41.170	37.182
C-F	74.415	70.538	59.296	42.525	25.062	14.789	13.343
C-S	227.130	220.137	197.980	157.598	102.449	63.045	57.126
C-C	270.760	264.222	243.284	202.966	140.318	89.329	81.255

Moreover, Table 10 and Figs. 4(a) and 4(b) present the fundamental frequency of LCSCBs with respect to the E_1/E_2 ratio. The results demonstrate that an increase in the E_1/E_2 ratio leads to higher frequencies for all boundary conditions and fiber angles.

Table 10. Fundamental frequencies ω (Hz) for LCSCBs ($L/h = 5; R/L = 5$) with respect to E_1/E_2 ratio

BCs	E_1/E_2						
	2	10	25	40	50	80	100
0°/45°							
S-S	48.855	84.772	120.609	143.634	155.382	180.983	193.142
C-F	17.556	30.872	45.008	54.762	60.009	72.249	78.536
C-S	74.238	123.403	165.789	189.509	200.681	223.279	233.399
C-C	109.171	176.832	232.271	263.703	279.232	313.794	331.530
0°/45°/0°							
S-S	52.618	108.689	155.796	181.857	194.011	218.078	228.462
C-F	18.955	40.357	60.523	73.138	79.521	93.375	99.962
C-S	79.645	151.978	199.656	221.898	231.619	250.385	258.613
C-C	116.361	208.714	265.305	294.020	308.097	340.253	357.448

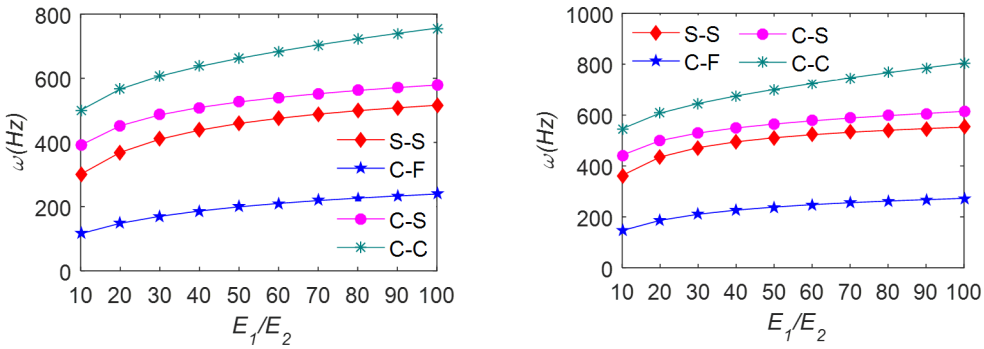

(a) (0°/45°) beam (b) (0°/45°/0°) beam

Figure 4. Fundamental frequencies ω (Hz) of the (0°/45°) and (0°/45°/0°) LCSCBs ($L/h = 5; R/L = 5$) with respect to E_1/E_2 ratio with various boundary conditions

The mode shapes of LCSCBs under S-S, C-F, C-S, and C-C boundary conditions are visually depicted in Figs. 5, 6, 7, and 8, respectively. Observation reveals that for C-F and S-S beams, the first

mode corresponds to a bending mode, while the second, third, and fourth modes indicate shearing modes. In contrast, the first four modes predominantly represent shearing modes for C-S and C-C beams. Notably, it is highlighted that the influence of shear effects is more pronounced in C-S and C-C beams compared to C-F and S-S beams.

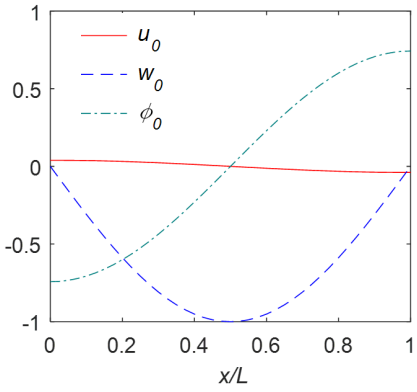

(a) Mode 1; ω_1 = 325.513 (Hz)

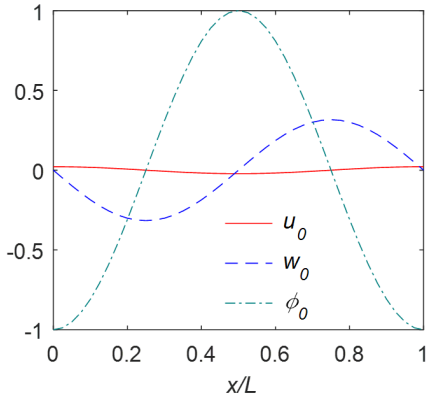

(b) Mode 2; ω_2 = 968.253 (Hz)

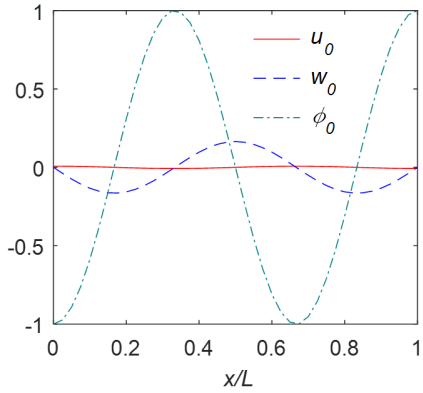

(c) Mode 3; ω_3 = 1689.444 (Hz)

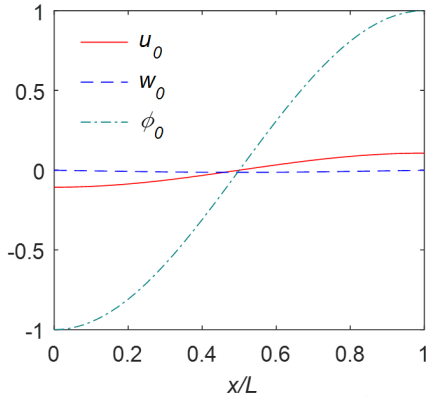

(d) Mode 4; ω_4 = 2435.305 (Hz)

Figure 5. First four mode shapes of S-S LCSCB ($0°/90°$; $L/h = 5$; $R/L = 5$)

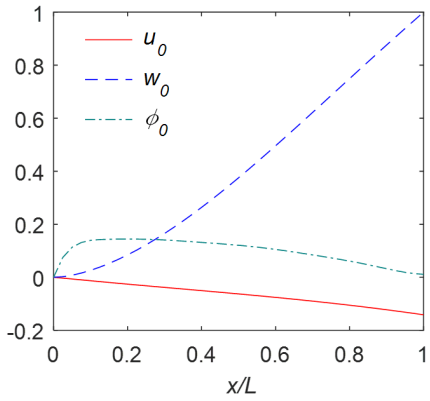

(a) Mode 1; ω_1 = 125.110 (Hz)

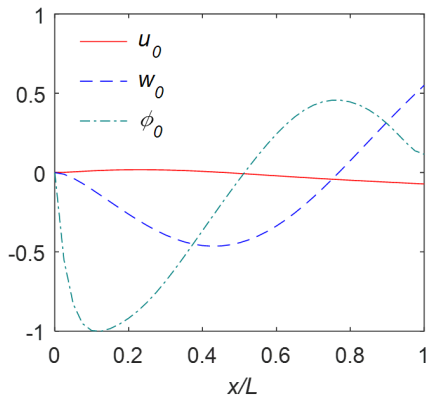

(b) Mode 2; ω_2 = 577.303 (Hz)

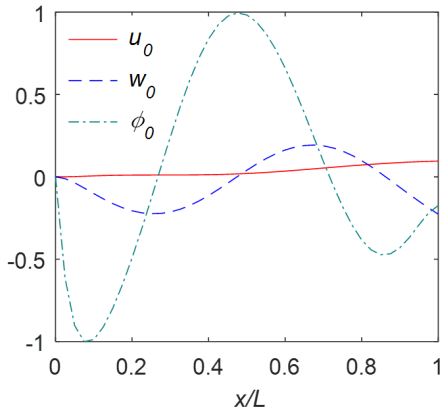

(c) Mode 3; ω_3 = 1249.593 (Hz)

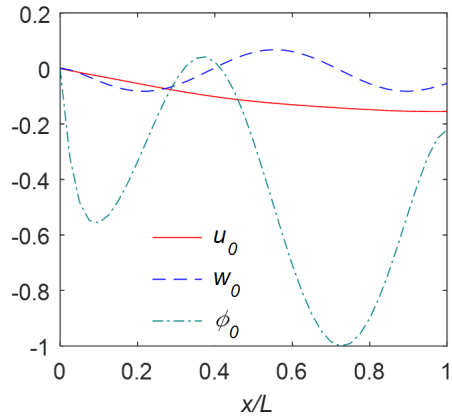

(d) Mode 4; ω_4 = 1659.874 (Hz)

Figure 6. First four mode shapes of C-F LCSCB ($0^\circ/90^\circ$; $L/h = 5$; $R/L = 5$)

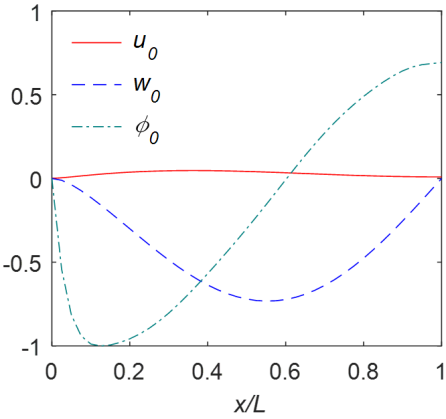

(a) Mode 1; ω_1 = 425.537 (Hz)

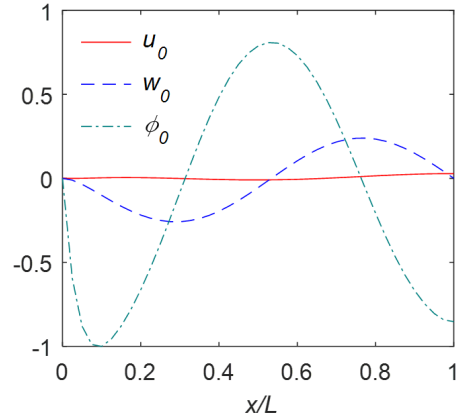

(b) Mode 2; ω_2 = 1056.698 (Hz)

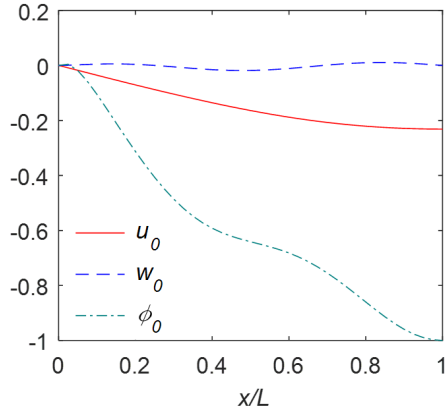

(c) Mode 3; ω_3 = 1627.069 (Hz)

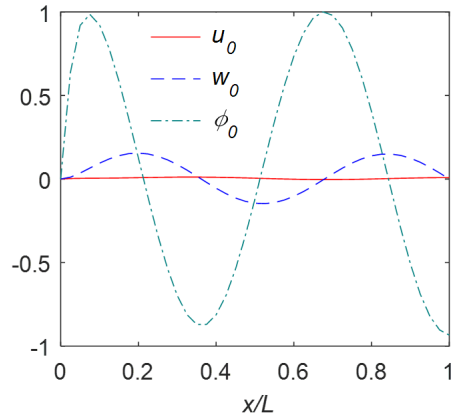

(d) Mode 4; ω_4 = 1779.950 (Hz)

Figure 7. First four mode shapes of C-S LCSCB ($0^\circ/90^\circ$; $L/h = 5$; $R/L = 5$)

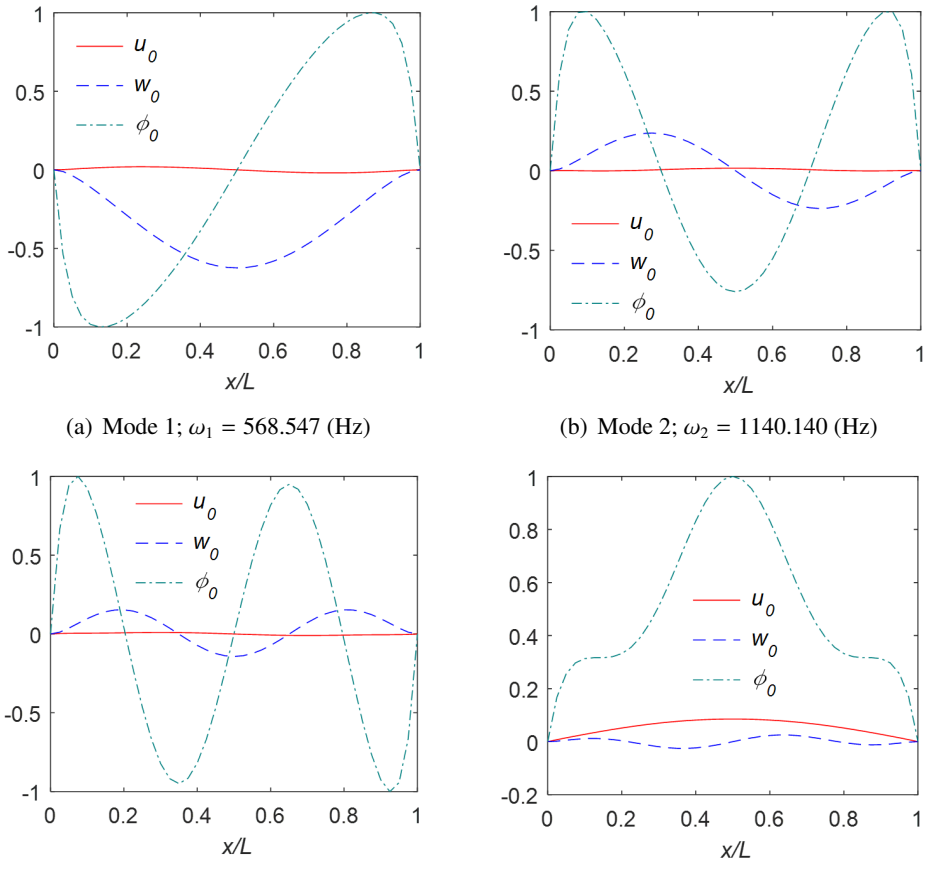

(a) Mode 1; ω_1 = 568.547 (Hz)

(b) Mode 2; ω_2 = 1140.140 (Hz)

(c) Mode 3; ω_3 = 1875.432 (Hz)

(d) Mode 4; ω_4 = 2424.602 (Hz)

Figure 8. First four mode shapes of C-C LCSCB ($0^\circ/90^\circ; L/h = 5; R/L = 5$)

4. Conclusions

The introduction of novel Ritz functions in this study provided a comprehensive framework for evaluating the free vibration characteristics of laminated composite shallow curved beams under diverse boundary conditions, emphasizing displacement based on the higher-order deformation beam theory. Furthermore, the governing equations were formulated utilizing Lagrange equations. The research delved into the impact of several parameters, including the length-to-thickness ratio, curvature ratio, fiber angle, material anisotropy, and boundary conditions on the natural frequency of the beams. Here are the key findings:

- A rise in the L/h ratio and fiber angle (θ) resulted in a decrease in the frequency of LCSCBs.
- An escalation in the E_1/E_2 ratio increased the frequency of LCSCBs.
- The variation in the R/L ratio had an insignificant impact on the frequency of LCSCBs.
- The frequencies were notably higher for C-C beams and lower for C-F beams.
- Overall, the current methodology demonstrates efficiency in analyzing the free vibration characteristics of LCSCBs.

References

[1] Qatu, M. S. (2004). Plates. In *Vibration of Laminated Shells and Plates*, Elsevier, 109–179.

[2] Li, J., Huo, Q., Li, X., Kong, X., Wu, W. (2013). Vibration analyses of laminated composite beams using refined higher-order shear deformation theory. *International Journal of Mechanics and Materials in Design*, 10(1):43–52.

[3] Adam, C., Ladurner, D., Furtmüller, T. (2022). Free and forced small flexural vibrations of slightly curved slender composite beams with interlayer slip. *Thin-Walled Structures*, 180:109857.

[4] Qatu, M. S. (1992). In-plane vibration of slightly curved laminated composite beams. *Journal of Sound and Vibration*, 159(2):327–338.

[5] Corrêa, R. M., Arndt, M., Machado, R. D. (2021). Free in-plane vibration analysis of curved beams by the generalized/extended finite element method. *European Journal of Mechanics - A/Solids*, 88:104244.

[6] Wu, J.-S., Chiang, L.-K. (2004). Free vibration of a circularly curved Timoshenko beam normal to its initial plane using finite curved beam elements. *Computers & Structures*, 82(29–30):2525–2540.

[7] Anh, P. H., Duong, T. T. (2019). Weight optimisation of functionally graded beams using modified differential evolution. *Journal of Science and Technology in Civil Engineering (STCE) - NUCE*, 13(2): 48–63.

[8] Lien, T. V., Khiem, N. T., Duc, N. T. (2016). Free vibration analysis of functionally graded Timoshenko beam using dynamic stiffness method. *Journal of Science and Technology in Civil Engineering (JSTCE)-HUCE*, 10(5):19–28.

[9] Avhad, P. V., Sayyad, A. S. (2021). On the deformation of laminated composite and sandwich curved beams. *Curved and Layered Structures*, 9(1):1–12.

[10] Javani, M., Kiani, Y., Eslami, M. R. (2019). Free vibration of arbitrary thick FGM deep arches using unconstrained higher-order shear deformation theory. *Thin-Walled Structures*, 136:258–266.

[11] Jun, L., Hongxing, H., Rongying, S. (2008). Free vibration of laminated composite circular arches by dynamic stiffness analysis. *Journal of Reinforced Plastics and Composites*, 27(8):851–870.

[12] Khdeir, A. A., Reddy, J. N. (1997). Free and forced vibration of cross-ply laminated composite shallow arches. *International Journal of Solids and Structures*, 34(10):1217–1234.

[13] Li, X., Guedes Soares, C. (2015). Spectral finite element analysis of in-plane free vibration of laminated composite shallow arches. *Composite Structures*, 132:484–494.

[14] Jun, L., Guangwei, R., Jin, P., Xiaobin, L., Weiguo, W. (2013). Free Vibration Analysis of a Laminated Shallow Curved Beam Based on Trigonometric Shear Deformation Theory. *Mechanics Based Design of Structures and Machines*, 42(1):111–129.

[15] Hung, D. X., Truong, H. Q. (2018). Free vibration analysis of sandwich beams with FG porous core and FGM faces resting on Winkler elastic foundation by various shear deformation theories. *Journal of Science and Technology in Civil Engineering (STCE) - NUCE*, 12(3):23–33.

[16] Arikoglu, A., Ozturk, A. G. (2020). A novel approach for in-plane vibration and damping analysis of arbitrarily curved laminated composite and sandwich beams. *Composite Structures*, 253:112781.

[17] Cevik, M. (2008). Effects of Fiber Orientation on Out-of-plane and In-plane Natural Frequencies of Angle-ply Laminated Composite Arches. *Journal of Reinforced Plastics and Composites*, 28(1):59–71.

[18] Marur, S. R., Kant, T. (2011). Transient dynamic analysis of higher order sandwich and composite arches. *Composite Structures*, 93(4):1201–1216.

[19] Yang, F., Sedaghati, R., Esmailzadeh, E. (2008). Free in-plane vibration of general curved beams using finite element method. *Journal of Sound and Vibration*, 318(4–5):850–867.

[20] Luu, A.-T., Kim, N.-I., Lee, J. (2015). NURBS-based isogeometric vibration analysis of generally laminated deep curved beams with variable curvature. *Composite Structures*, 119:150–165.

[21] Tseng, Y. P., Huang, C. S., Kao, M. S. (2000). In-plane vibration of laminated curved beams with variable curvature by dynamic stiffness analysis. *Composite Structures*, 50(2):103–114.

[22] Matsunaga, H. (2004). Free vibration and stability of laminated composite circular arches subjected to initial axial stress. *Journal of Sound and Vibration*, 271(3–5):651–670.

[23] Yasin, M. Y., Khalid, H. M., Beg, M. S. (2020). Exact solution considering layerwise mechanics for laminated composite and sandwich curved beams of deep curvatures. *Composite Structures*, 244:112258.

[24] Thang, N. T., Long, N. V., Tu, T. M., Nam, N. H., Anh, M. C. (2022). Navier solution for static and free vibration analysis of sandwich plate with auxetic honeycomb core resting on pasternak elastic foundation.

Journal of Science and Technology in Civil Engineering (STCE) - HUCE, 16(3):18–28.

[25] Aydogdu, M. (2005). Vibration analysis of cross-ply laminated beams with general boundary conditions by Ritz method. *International Journal of Mechanical Sciences*, 47(11):1740–1755.

[26] Khodabakhshpour-Bariki, S., Jafari-Talookolaei, R.-A., Attar, M., Eyvazian, A. (2021). Free vibration analysis of composite curved beams with stepped cross-section. *Structures*, 33:4828–4842.

[27] Mantari, J. L., Canales, F. G. (2016). Free vibration and buckling of laminated beams via hybrid Ritz solution for various penalized boundary conditions. *Composite Structures*, 152:306–315.

[28] Nguyen, T.-K., Nguyen, N.-D., Vo, T. P., Thai, H.-T. (2017). Trigonometric-series solution for analysis of laminated composite beams. *Composite Structures*, 160:142–151.

[29] Karamanli, A., Wattanasakulpong, N., Lezgy-Nazargah, M., Vo, T. P. (2023). Bending, buckling and free vibration behaviours of 2D functionally graded curved beams. *Structures*, 55:778–798.

[30] Marur, S. R., Kant, T. (2008). Free vibration of higher-order sandwich and composite arches, Part I: Formulation. *Journal of Sound and Vibration*, 310(1–2):91–109.

[31] Qatu, M. S., Elsharkawy, A. A. (1993). Vibration of laminated composite arches with deep curvature and arbitrary boundaries. *Computers & Structures*, 47(2):305–311.

[32] Yousefi, A., Rastgoo, A. (2011). Free vibration of functionally graded spatial curved beams. *Composite Structures*, 93(11):3048–3056.

[33] Pham, S. D., Karamanli, A., Wattanasakulpong, N., Vo, T. P. (2024). A Quasi-3D theory for bending, vibration and buckling analysis of FG-CNTRC and GPLRC curved beams. *Structures*, 63:106431.

[34] Qatu, M. S. (1993). Theories and analyses of thin and moderately thick laminated composite curved beams. *International Journal of Solids and Structures*, 30(20):2743–2756.

[35] Nguyen, N.-D., Nguyen, T.-N., Nguyen, T.-K., Vo, T. P. (2023). A Chebyshev–Ritz solution for size-dependent analysis of the porous microbeams with various boundary conditions. *International Journal of Mechanics and Materials in Design*, 19(4):861–881.

[36] Duong, N. N., Kien, N. T., Nhan, N. T. (2019). Ritz solution for buckling analysis of thin-walled composite channel beams based on a classical beam theory. *Journal of Science and Technology in Civil Engineering (STCE) - NUCE*, 13(3):34–44.

[37] Gupta, V. K., Panwar, Y. K., Sikhwal, O. (2012). Generalized Fibonacci Sequences. *Theoretical Mathematics and Applications*, 2(2):115–124.

[38] Mohamed, S. A., Mohamed, N., Eltaher, M. A. (2022). Bending, buckling and linear vibration of bio-inspired composite plates. *Ocean Engineering*, 259:111851.

[39] Timorian, S., Petrone, G., De Rosa, S., Franco, F., Ouisse, M., Bouhaddi, N. (2019). Spectral analysis and structural response of periodic and quasi-periodic beams. *Proceedings of the Institution of Mechanical Engineers, Part C: Journal of Mechanical Engineering Science*, 233(23–24):7498–7512.